The EMBO Journal (2010) 29, 3118–3129 | © 2010 European Molecular Biology Organization | All Rights Reserved 0261-4189/10
www.embojournal.org

THE EMBO JOURNAL

Crystal structure of a transfer-ribonucleoprotein particle that promotes asparagine formation

Mickaël Blaise[1,*], Marc Bailly[2], Mathieu Frechin[2], Manja Annette Behrens[3], Frédéric Fischer[2], Cristiano LP Oliveira[3,4], Hubert Dominique Becker[2], Jan Skov Pedersen[3], Søren Thirup[1] and Daniel Kern[2,*]

[1]Department of Molecular Biology, CARB Centre, University of Aarhus, Århus C, Denmark, [2]Institut de Biologie Moléculaire et Cellulaire, UPR 9002 du CNRS, Architecture et Réactivité de l'ARN, Université de Strasbourg, Strasbourg, Cedex, France and [3]Department of Chemistry, iNANO Interdisciplinary Nanoscience Center, University of Aarhus, Århus C, Denmark

Four out of the 22 aminoacyl-tRNAs (aa-tRNAs) are systematically or alternatively synthesized by an indirect, two-step route requiring an initial mischarging of the tRNA followed by tRNA-dependent conversion of the non-cognate amino acid. During tRNA-dependent asparagine formation, $tRNA^{Asn}$ promotes assembly of a ribonucleoprotein particle called transamidosome that allows channelling of the aa-tRNA from non-discriminating aspartyl-tRNA synthetase active site to the GatCAB amidotransferase site. The crystal structure of the *Thermus thermophilus* transamidosome determined at 3 Å resolution reveals a particle formed by two GatCABs, two dimeric ND-AspRSs and four $tRNAs^{Asn}$ molecules. In the complex, only two tRNAs are bound in a functional state, whereas the two other ones act as an RNA scaffold enabling release of the asparaginyl-$tRNA^{Asn}$ without dissociation of the complex. We propose that the crystal structure represents a transient state of the transamidation reaction. The transamidosome constitutes a transfer-ribonucleoprotein particle in which tRNAs serve the function of both substrate and structural foundation for a large molecular machine.

The EMBO Journal (2010) **29,** 3118–3129. doi:10.1038/emboj.2010.192; Published online 17 August 2010
Subject Categories: proteins; structural biology
Keywords: crystal structure; indirect tRNA asparaginylation; transamidosome; transfer-ribonucleoprotein particle; tRNA scaffold

*Corresponding authors. M Blaise, Department of Molecular Biology, CARB Centre, University of Aarhus, Gustav Wieds Vej, 10 c, DK-8000 Århus C, Denmark. Tel.: +45 8942 5265; Fax: +45 8612 3178; E-mail: mickael.blaise@gmail.com or D Kern, Institut de Biologie Moléculaire et Cellulaire, UPR 9002 du CNRS, 15, rue René Descartes, F-67084 Strasbourg, Cedex, France. Tel.: +33 (0)3 88 41 70 92; Fax: +33 (0)3 88 60 22 18; E-mail: d.kern@ibmc-cnrs.unistra.fr
[4]Present address: Complex Fluids Group, Department of Experimental Physics, University of São Paulo, São Paulo 05314-970, Brazil

Received: 14 April 2010; accepted: 15 July 2010; published online: 17 August 2010

Introduction

The fidelity of translation depends on accurate synthesis of aminoacyl-tRNAs (aa-tRNAs) by the aa-tRNA synthetases (aaRS). Eighteen of the 22 species of homologous aa-tRNAs participating in protein synthesis are formed by direct charging of the amino acid (aa) onto the cognate tRNA. In contrast, the cognate aa-tRNAs pairs charged with asparagine (Asn), glutamine (Gln), selenocysteine (Sec) and cysteine (Cys) are systematically (Sec) or alternatively (Asn, Gln and Cys) formed by a two-step process (Ibba and Söll, 2004; Kern *et al*, 2005; Sheppard *et al*, 2008). In these alternative pathways, the cognate aa-tRNA is formed by conversion of an esterified non-cognate amino acid (aa) first attached on the tRNA by a non-cognate aaRS (Curnow *et al*, 1996, 1998; Becker and Kern, 1998). This pathway raises the question of how the mischarged aa-tRNA intermediate travels from the aaRS to the aa-modifying enzyme. This process must prevent both, the use of the mischarged aa-tRNA in protein synthesis as well as the hydrolysis of the very labile ester bond linking the aa to the tRNA. Recently, we have unraveled the coupling of the two steps of indirect asparaginyl-$tRNA^{Asn}$ (Asn-$tRNA^{Asn}$) formation in *Thermus thermophilus* in which the aspartate (Asp) mischarged onto $tRNA^{Asn}$ by a non-discriminating aspartyl-tRNA synthetase (ND-AspRS) is amidated into Asn by a GatCAB tRNA-dependent amidotransferase (Bailly *et al*, 2007). Both enzymes, together with the uncharged tRNA assemble into a ribonucleoprotein particle (RNP) called transamidosome in which the mischarged Asp-$tRNA^{Asn}$ formed by the ND-AspRS is channelled to the GatCAB that amidates the Asp esterified on the $tRNA^{Asn}$ (Bailly *et al*, 2007). The assembly of the three partners prevents both the hydrolysis of the labile, mischarged aa-tRNA intermediate and its premature release that could potentially challenge the integrity of the genetic code (Bailly *et al*, 2007).

Given the necessity of the transamidosome for faithful translation of Asn codons, there is a possibility that all so-called indirect pathways of aa-tRNA formation might systematically use particles in which the tRNA, the mischarging aaRS and the aa-modifying enzyme assemble. Indeed, it was recently shown that in methanogenic archaea, tRNA cysteinylation is catalysed by a particle in which the $tRNA^{Cys}$ substrate is bound to O-phosphoseryl-tRNA synthase (SepRS) and Sep-tRNA•Cys-tRNA synthase (SepCysS) that form Cys-$tRNA^{Cys}$ (Zhang *et al*, 2008). Likewise, in mammals, tRNA selenocysteinylation proceeds through formation of supramolecular complexes including the partners that promote formation of Sec-$tRNA^{Sec}$, $tRNA^{Sec}$ modification and incorporation of Sec into polypeptide chains (Small-Howard *et al*, 2006).

Discovery of transfer-ribonucleoprotein (tRNP) particles in which tRNA might act as a scaffold raises a wide range of new structural and functional issues concerning the assembly of the protein and nucleic acid partners, such as the recruitment of the specific substrate by the non-discriminating

aaRS, and the mechanism of channelling of the mischarged aa-tRNA from one active site to the other one. To gain insights into which structural elements are involved in the assembly of these tRNPs and in channelling of the aa-tRNA inside these particles, we solved the 3D structure of the *T. thermophilus* transamidosome by X-ray crystallography and its structure in solution by small angle X-ray scattering (SAXS). The crystal structure represents a transient state of the transamidation reaction. The structural and biochemical data reveal a particle in which the four-bound $tRNAs^{Asn}$ have two different non-overlapping functions: two are substrates and cofactors for Asn formation, whereas the two others constitute catalytically inert but essential building blocks bricks of this molecular machine. The $tRNA^{Asn}$ stabilizes indeed the transamidosome to prevent release of the mischarged aa-tRNA intermediate and also to prevent the GatCAB denaturation at the optimal growth temperature of *T. thermophilus*. The crystal structure reveals how the ND-AspRS accommodates the $tRNA^{Asn}$ anticodon and suggests that the tRNA acceptor carrying the mischarged Asp undergoes a 35-Å shift to switch from the aminoacylation to the transamidation active site of the tRNP.

Results

Crystal structure of the transamidosome

The structure of the complex was solved by molecular replacement as described (Bailly *et al*, 2009). The refinement statistics are shown in Table I. The asymmetric unit contains a 520-kDa complex formed by two dimeric ND-AspRSs, two trimeric GatCABs and four $tRNAs^{Asn}$ (Figure 1A–C). The structure of the ND-AspRS resembles those described for other bacterial and eukaryotic AspRSs (Ruff *et al*, 1991; Delarue *et al*, 1994). Each subunit of the homodimer contains two main domains. The C-terminal (C-t) catalytic core, organized as a seven-stranded antiparallel β-sheet including the three consensus motifs of class II aaRSs (Charron *et al*, 2003), catalyses both the activation of Asp in the presence of ATP and its transfer onto the 3′ OH ribose of the terminal adenosine of $tRNA^{Asn}$. The N-terminal (N-t) anticodon-binding domain (ABD) is an OB fold formed by a five-stranded β-barrel (Charron *et al*, 2003) (Figure 1). The two domains are linked by a 20-aa-long hinge region essential for the aminoacylation activity, as it ensures inter-domain communication and dimerization of the subunits (Ruff *et al*, 1991; Delarue *et al*, 1994). The organization of *T. thermophilus* GatCAB resembles that of the enzymes from *Staphylococcus aureus* and *Aquifex aeolicus* (Nakamura *et al*, 2006, 2010; Wu *et al*, 2009). The core of the GatA subunit, which exhibits the amidohydrolase activity, is organized as an 11-stranded β-sheet mixed with α-helices. GatB is formed by two domains connected by a long loop. The N-t part forms a globular cradle domain and the C-t an α-helical domain named Yqey. However, because of the lack of clear electron density, the Yqey domain has been traced as a polyalanine chain (Figure 1E; Supplementary Figure S1). Notably, an anomalous signal peak was detected in each GatB subunit and attributed to a zinc ion tetrahedrally coordinated by residues Cys22, Cys24, Cys38 and Cys41 (Supplementary Figure S2). The zinc ion seems to contribute to the stability of the complex and to the organization of the ammonia channel crossing the GatA and GatB subunits. This channel ensures the transfer of the ammonium ions formed in the amidase site of GatA to the transamidase site of GatB (Nakamura *et al*, 2006). Finally, the contact area between GatA and GatB is surrounded by GatC, previously described as a chaperone, which forms a belt attaching the two subunits (Figure 1). The four tRNAs of the tRNP display two different binding modes to the GatCABs. The so-called catalytic $tRNA^{Asn}$ ($_{cat}tRNA^{Asn}$) are bound in a functional state with their anticodon loops contacting the ABD of one of the monomers of the ND-AspRS and their acceptor arms buried in the GatB active site of the GatCABs. Both $_{cat}tRNAs^{Asn}$ bind the GatCAB and ND-AspRS molecules in the same manner (Figure 1C–F). The second tRNA-binding mode is adopted by the so-called scaffolding $tRNAs^{Asn}$ ($_{scaf}tRNA^{Asn}$), which binds in a non-catalytic manner. Although their anticodon loops bind the ABD of the other ND-AspRS monomer, their acceptor stems are entrapped in the interface between the GatA and GatB subunits of the second GatCAB molecule. Both $_{scaf}tRNAs^{Asn}$ bind the GatCAB and ND-AspRS molecules in a same manner (Figure 1C–F). This means that in the complex each GatCAB binds one $_{scaf}tRNA^{Asn}$ and one $_{cat}tRNA^{Asn}$ (Figure 1D). Because of the lack of a clear electron density, the 3′ OH-CCA end of $_{scaf}tRNAs^{Asn}$ was not built. Only a limited number of protein–protein contacts could be observed between the ND-AspRS and the GatCAB. Each GatCAB interacts with the two surrounding ND-AspRS monomers; Arg110, Arg111 and Arg113 from the GatB subunit contact Ser320, Ala365, Lys366, Gly367, from the ND-AspRS monomer by H-bonds or Van der Waals interactions and Glu130, Gly131 and Ala132

Table I Data collection and refinement statistics

Data collection[a]	
Beamline	X10SA, Swiss Light Source
Wavelength (Å)	0.98
Space group	$P2_1$
Resolution (Å)	50-3
Cell dimensions	
a, *b*, *c* (Å)	$a=115.9$, $b=214.0$, $c=127.8$
α, β, γ (deg)	$\alpha=90$, $\beta=93.3$, $\gamma=90$
Resolution (Å)	50-3
R_{meas}	15.4 (80.5)
$R_{mrgd\text{-}F}$	14 (63.9)
$(I/\sigma(I))$	10.3 (2.4)
Completeness (%)	99.9 (99.9)
Redundancy	4.25
Refinement	
Resolution (Å)	39.18-3.00
No. of reflections	123 924
R_{work}/R_{free} (%)	21.1/25.1
No. of atoms	33 548
Protein	27 186
Nucleic acids	6224
Ions Mg/Zn	29/2
Water	107
B-factors	
Protein overall	49.2
Nucleic acids overall	66.2
Ions Mg/Zn	28.3/63.6
Water	56.6
R.m.s.d.	
Bond lengths (Å)	0.01
Bond angles (deg)	0.95
Ramachandran plot[b] *(%)*	
In core	92.2
Allowed	7.3

[a]Values in parenthesis are for the last resolution shell.
[b]Values are from Molprobity.

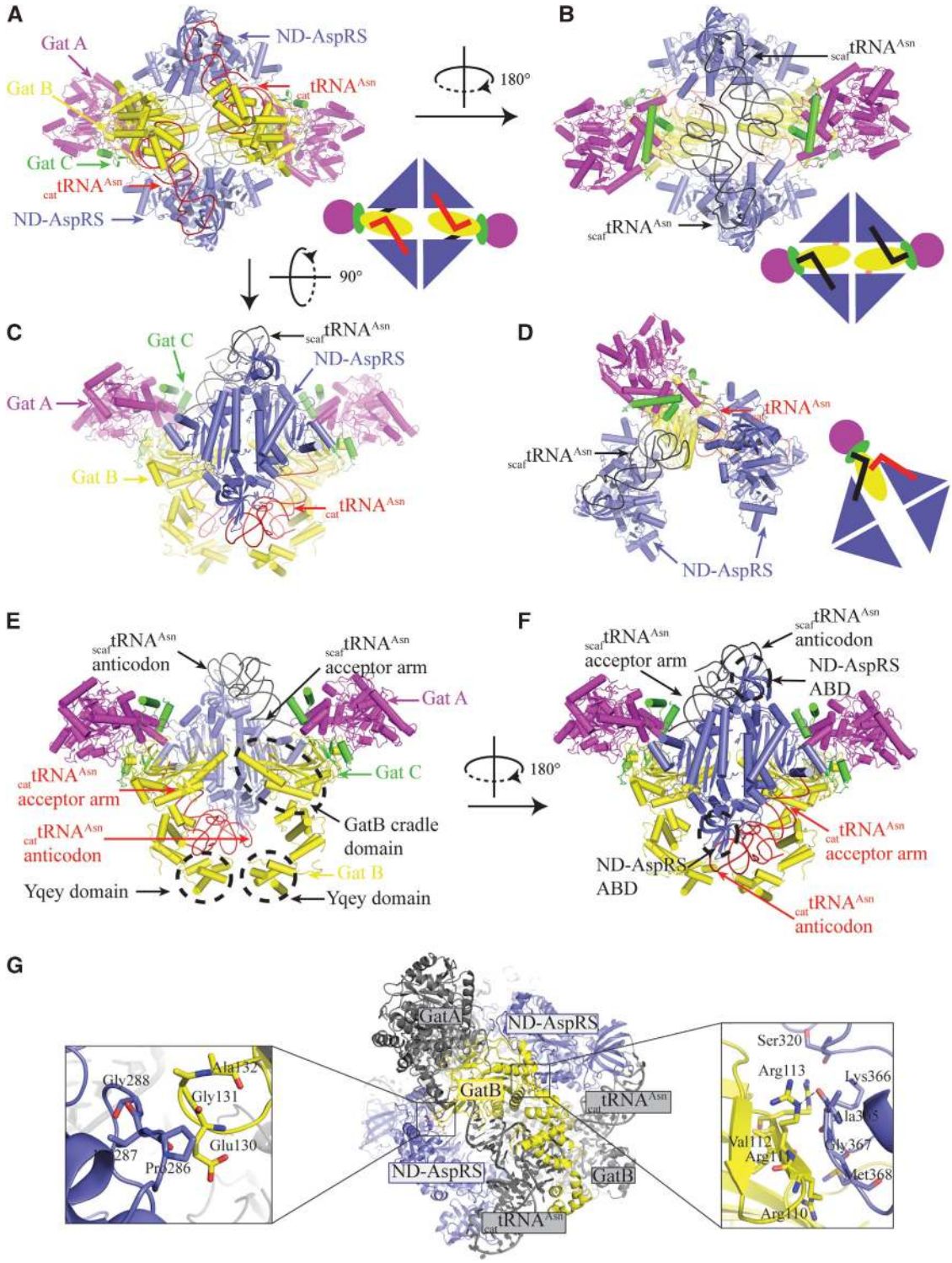

Figure 1 Crystal structure of the transamidosome. (**A**–**C**) Composition of the asymmetric unit. The ND-AspRS appears in blue, the $_{cat}$tRNA^{Asn} in red, the $_{scaf}$tRNA^{Asn} in grey and the subunits of the trimeric GatCAB in green, magenta and yellow. The schematic structure follows the same colour code. (**D**) On this view, one GatCAB, one $_{scaf}$tRNA^{Asn} and one $_{cat}$tRNA^{Asn} have been removed, to show that each ND-AspRS binds one $_{scaf}$tRNA^{Asn} and one $_{cat}$tRNA^{Asn} in order to recruit one GatCAB. (**E**, **F**) Structure of the transamidosome in which one ND-AspRS, one $_{cat}$tRNA^{Asn} and one $_{scaf}$tRNA^{Asn} have been removed and which corresponds to that in solution. The dotted circles indicate the GatB catalytic (cradle) and Yqey domains and the ND-AspRS ABD. (**G**) Protein–protein interactions in the transamidosome. All the components are in grey, except GatB and the two ND-AspRSs that appear, respectively, in yellow and blue. The panels show a zoom of the two regions of GatB and the ND-AspRS in contact and the residues involved in the interaction; the hydrogen bond is indicated by the dashed line.

from the same GatB contact residues 286–288 of the other ND-AspRS monomer, by Van der Waals interactions (Figure 1G). However, as previously demonstrated, these few protein–protein interactions are not sufficient to mediate complex formation in the absence of tRNA (Bailly *et al*, 2007).

Comparison between the crystal structure and the structure in solution determined by SAXS

The composition of the transamidosome in solution was previously investigated by size exclusion chromatography, static light scattering, dynamic light scattering and analytical ultracentrifugation (Bailly *et al*, 2008). All these approaches have predicted a molecular weight for the transamidosome ranging from 300 to 400 kDa, in agreement with a 380-kDa complex, composed of one dimeric ND-AspRS, two tRNAs^{Asn} and two GatCABs but in contradiction with the crystal structure showing the presence of an extra ND-AspRS bound to two tRNAs^{Asn}. Thus, to gain insights into the stoichiometry of the macromolecules that compose the transamidosome in solution, we investigated the particle by SAXS. The pair distribution function $p(r)$ obtained by an indirect Fourier transformation of the experimental SAXS data shows that the transamidosome in solution is an elongated particle with a maximal diameter of 185 Å. The SAXS data give a molecular mass of 325 ± 50 kDa and a radius of gyration of 55 ± 1 Å (Supplementary Figure S3). The size of the model obtained by *ab initio* methods (Figure 2A and B) suggests that the complex in solution consists, as shown previously, of one dimeric ND-AspRS, two GatCABs and two tRNAs. This is further confirmed by the comparison of the calculated scattering curves for various stoichiometries of the partners with the SAXS data, which gives the best fit for the 380-kDa model (Supplementary Figure S4).

The position of the two GatCABs and the presence of the $_{scaf}$tRNA^{Asn} in the crystal structure are surprising, as we were expecting that, as proposed previously, each ND-AspRS would bind two $_{cat}$tRNA^{Asn} and that the two GatCABs would be bound symmetrically to these tRNAs (Bailly *et al*, 2007). Thus, we compared the scattering curves for several models with the SAXS data. The theoretical scattering intensity calculated from the crystal structure of the transamidosome composed of one ND-AspRS bound to one $_{scaf}$tRNA^{Asn}, one $_{cat}$tRNA^{Asn} and two GatCABs gives a reasonable fit to the scattering data ($\chi = 6.8$) (Figure 2C and D). In contrast, the theoretical scattering intensity of a model in which the two tRNAs^{Asn} are bound catalytically on the dimeric ND-AspRS and the two GatCABs are equivalent and symmetrical gives a poor fit ($\chi = 8$) compared with the model extracted from the crystal structure (Figure 2E and F). As proposed previously, the C-t domain of the GatB subunit may be flexible in the absence of tRNA (Nakamura *et al*, 2006, 2010). We therefore performed rigid body refinement, using the SASREF program (Svergun and Petoukhov, 2005), in order to fit the GatB C-t domain, with the scattering data. A reasonable fit ($\chi = 3.4$) was obtained with a model in which the C-t domain of one GatB shifts closer to the GatB catalytic domain, whereas that of the other GatB is anchored to the bound tRNA^{Asn}. Thus, one of the two GatB C-t domain is not bound to tRNA (Figure 2G and H).

Altogether, the SAXS results clearly indicate that in solution the transamidosome comprises one ND-AspRS, two GatCABs and two tRNAs^{Asn}. But as the χ value from model extracted from crystal structure fits with the SAXS data, the results agree with non-equivalent orientations of the two GatCABs. Finally, the rigid body refinement shows that one of the two GatBs has its C-t flexible and therefore it does not bind tRNA in its active site in solution. This tRNA is the $_{scaf}$tRNA^{Asn}. To confirm these observations, we investigated the equivalence of the tRNAs^{Asn} by kinetic experiments.

GatCAB takes control of the ND-AspRS catalytic mode inside the tRNP

Aminoacylation of tRNA^{Asn} by the preformed ND-AspRS•tRNA^{Asn} complex, in the absence of free tRNA, shows a homogeneous hyperbolic kinetic and formation of two Asp-tRNA^{Asn} with identical rate constants. Thus, both catalytic sites of the dimeric ND-AspRS are equivalent (Figure 3A). The rate constant equals that of tRNA charging at the steady state when free tRNA^{Asn} is added in excess (Figure 3A). In contrast, in the preformed ternary ND-AspRS•tRNA^{Asn}•GatCAB complex, aminoacylation of tRNA^{Asn} occurs through a biphasic kinetic formed by a hyperbolic fast phase followed by a significantly slower linear phase (Figure 3B). The slow linear phase extrapolates at t_o to one Asp-tRNA^{Asn} formed per dimeric ND-AspRS. The amplitude of the burst increases linearly with the concentration of the transamidosome (not shown) but is not altered in the presence of an excess of free tRNA^{Asn} (Figure 3B). As the rate constants derived from two phases differ by two orders of magnitude (respectively, 0.19 and 0.0018/s; Figure 3B), the stoichiometry of one aa-tRNA formed in the burst by the two active sites of the dimeric ND-AspRS indicates that inside the transamidosome, the AspRS charges one tRNA^{Asn} faster than the second one (Kern and Lapointe, 1979). Thus, the kinetic of Figure 3B is consistent with a non-equivalence of the two tRNA^{Asn} aminoacylation sites of the ND-AspRS triggered by GatCAB binding that contrasts with the equivalent sites displayed by the free enzyme (Figure 3A). With respect to the structure of the transamidosome showing that the ND-AspRS binds one tRNA in a functional state but not the other one ($_{cat}$tRNA^{Asn} and $_{scaf}$tRNA^{Asn}), the biphasic kinetic could reflect the aminoacylation of the two non-equivalently bound tRNA^{Asn} by suggesting that, after fast aspartylation of $_{cat}$tRNA^{Asn}, followed by amidation of the Asp moiety, the $_{scaf}$tRNA^{Asn} is aspartylated slowly with the rate constant equaling that of the binary ND-AspRS•tRNA^{Asn} complex (Figure 3A). Therefore, we propose a working model of the transamidation reaction in which the large complex observed in the crystal structure would represent a transient state of the catalytic process and a snapshot of the transamidation reaction in which two ND-AspRSs saturated with tRNA^{Asn} are bound together to two GatCABs, one of the two ND-AspRS is leaving the complex while the second one is binding to it (Figure 3C). As this complex is not seen in solution, likely binding of a second ND-AspRS•tRNA^{Asn} complex provokes the release of the first one. According to the kinetic investigation, the leaving complex contains the Asn-$_{cat}$tRNA^{Asn} end product and the $_{scaf}$tRNA^{Asn}, whereas the entering one is saturated with uncharged tRNA^{Asn}.

What happens with the released ND-AspRS•tRNA^{Asn} complex? As most homologous aa-tRNAs, Asn-tRNA^{Asn} is trapped by the elongation factor EF-Tu and exchanged on the ND-AspRS with free tRNA^{Asn}. The $_{scaf}$tRNA^{Asn} either remains bound on AspRS or is exchanged with another molecule. Thus, a new complex forms in which the ND-AspRS binds equivalently the two tRNA^{Asn}. The strong affinity of tRNA^{Asn}-bound ND-AspRS for GatCAB (Bailly *et al*, 2007) promotes then binding of the complex on the preformed transamidosome (Figure 3C, steps 4–5) or on free GatCABs to form a new transamidosome, whether the concentration of GatCAB is limiting or exceeds that of the ND-AspRS, respectively. The previous $_{scaf}$tRNA^{Asn} can then bind functionally and become

catalytic. If $tRNA^{Asn}$ is aspartylated before entry of the ND-AspRS complex in the transamidosome, the poor affinity of the aspartylated $tRNA^{Asn}$ for EF-Tu with respect to the ND-AspRS contrasting with its strong affinity when bound on the ND-AspRS for GatCAB will considerably restrict its use for protein synthesis.

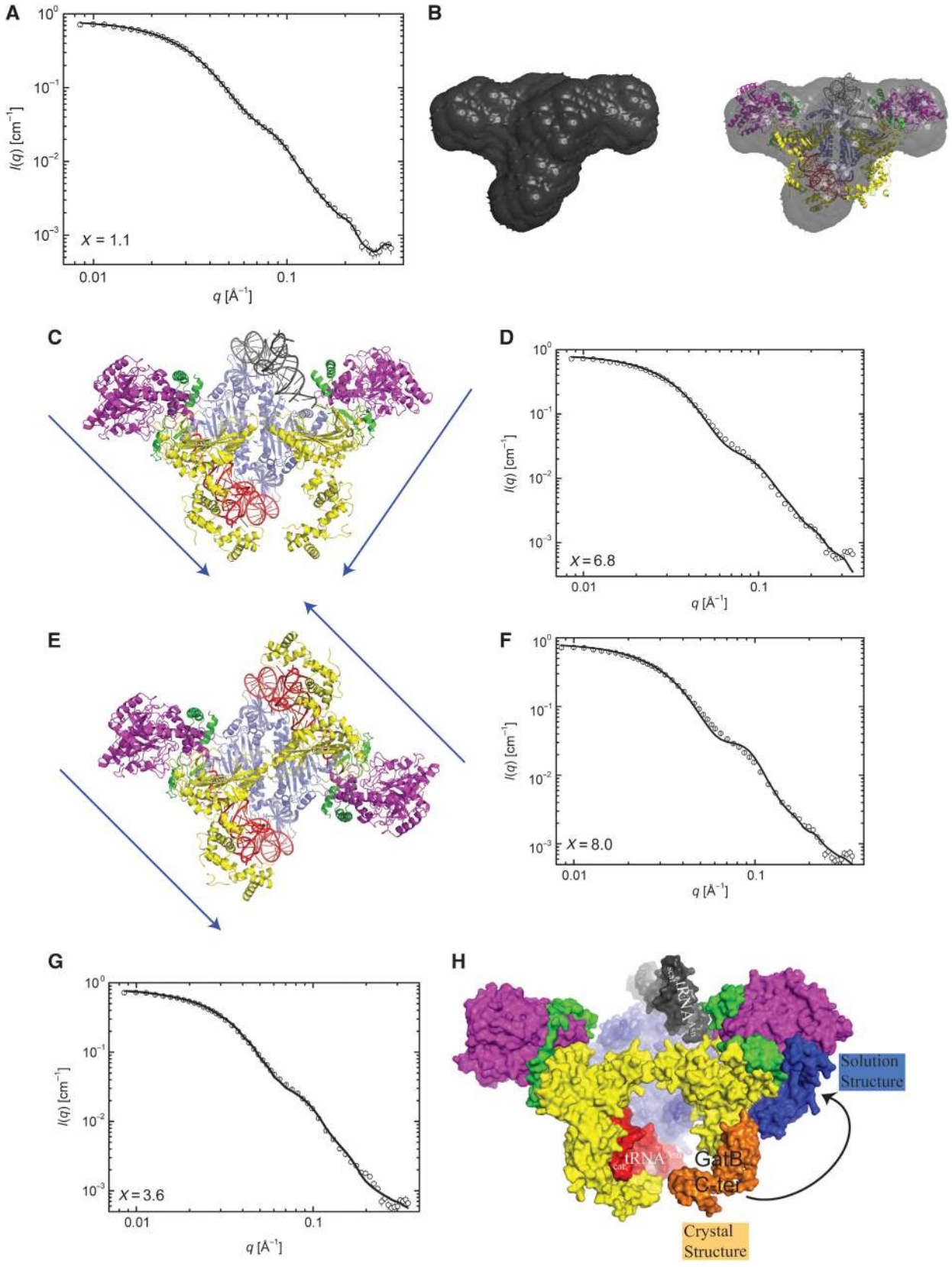

Structural basis of the non-discriminating behaviour of the AspRS

The ND-AspRS aspartylates both $tRNA^{Asp}$ and $tRNA^{Asn}$ with similar efficiencies (Becker and Kern, 1998). The structure of the transamidosome reveals how the enzyme accommodates both the 34GU**C36** anticodon of $tRNA^{Asp}$ and the 34GU**U36** anticodon of $tRNA^{Asn}$. Previous investigations have suggested that conformation of the L1-loop, connecting strands 4 and 5 of the ABD, is the key element that determines the relaxed specificity towards nucleotide 36 that distinguishes the two anticodons (Schmitt *et al*, 1998; Charron *et al*, 2003). Biochemical investigations have revealed that the *T. thermophilus* ND-AspRS uses G34 and U35 of $tRNA^{Asp}$ as major identity determinants for recognition but not C36, whereas all three nucleotides contribute strongly to recognition by the discriminating AspRS (Kern *et al*, 2005). Analysis of the interactions between ND-AspRS and $tRNA^{Asn}$ in the transamidosome shows that contacts are made between the ABD and all three nucleotides of the anticodon. The structure of the complex shows that G34 N1 establishes hydrogen bond with the Glu76 carboxyle group, whereas G34 N2 contacts both Asn68 Oδ1 and the carboxyle group of Glu76. In addition, U35 interacts with N3 and O4 of the Gln44 amide group and is involved in a stacking interaction with Phe33 (Figure 4A). Finally, the N3 and the ribose groups of U36 interact, respectively, with the Lys70 carbonyl and the Arg26 guanidinium groups. In the case of $tRNA^{Asp}$, which has a cytosine at position 36, the same interactions can still be formed explaining why the ND-AspRS cannot discriminate between $tRNA^{Asp}$ and $tRNA^{Asn}$.

GatB discriminates between $tRNA^{Asp}$ and $tRNA^{Asn}$ by recognizing U1 and measuring the D-loop length

The D- and T-loops as well as the T-stem of $_{cat}tRNA^{Asn}$ interact with the α-helical C-t part of GatB (Figure 4B). Recognition of the two loops is based on a shape complementarity, as described for tRNA binding by the CCA-adding enzyme and the GatDE amidotransferase (Oshikane *et al*, 2006; Tomita *et al*, 2006). The GatB C-t part forms a concave area, which hosts the T-stem loop (Figure 4B). Even though no side chains could be attributed to the Yqey domain residues, the structure suggests that this domain has a crucial function in tRNA binding, as helix 15 contacts nucleotide D20 and helix 16 is entrapped between nucleotides in positions 19 and 20. According to the SAXS data, the GatB C-t domain is flexible (not shown), in agreement with previous results that revealed the flexibility of the Yqey domain (Nakamura *et al*, 2006, 2010; Oshikane *et al*, 2006; Deniziak *et al*, 2007). This suggests that upon binding of GatCAB, the Yqey domain shifts to anchor the tRNA.

Previous biochemical investigations showed that the U1-A72 base-pair and more particularly nucleotide U1 constitutes the major $tRNA^{Asn}$ identity element for transamidation of the bound Asp by GatCAB. Substitution of the first base-pair of $tRNA^{Asn}$ with the G1-C72 pair prevents amidation of $tRNA^{Asn}$-bound Asp (Bailly *et al*, 2006). The crystal structure shows that U1-A72 is in the vicinity of the 3_{10} turn formed by residues 179–182, with U1 being tightly bound by Glu181 of GatB. The N atom from the main chain of Glu181 recognizes the O2 from the U1 ring, whereas its side chain contacts the ribose group. The recognition is achieved by interaction of the 5′ terminal phosphate of tRNA with the side chains of Ser211 and Arg160 as well as the amino group of Lys213. Finally, Pro180 and Phe212 are in close proximity of U1 and may act as a stop for positioning U1, while A72 is contacted by any residue (Figure 4C).

$_{cat}tRNA^{Asn}$ 3′ end recognition by the transamidation catalytic site

The GatB and AspRS active sites are separated from each other by a distance of about 40 Å. The model of the ND-AspRS bound to tRNA with the CCA-3′OH tRNA end in the AspRS active site demonstrates that the acceptor arm of $_{cat}tRNA^{Asn}$ has to shift 35 Å from the ND-AspRS to the GatB active site after aminoacylation (Figure 5A). The 3′ end of $_{cat}tRNA^{Asn}$ is deeply pushed into the GatB cradle domain (Figure 5B; Supplementary Figure S5). The terminal A76 sits in a pocket formed by Tyr81, Tyr83 and Tyr262, and its ribose ring contacts the Asp85 carboxyle group. Recognition is achieved by contacts established by C75, C74 and G73. The base ring of C75 interacts with the His128 imidazole and the Ser126 OH groups, whereas the phosphate contacts the Arg139 and Arg186 guanidinium groups. The C74 ring interacts, through the O2, with the Asn210 amide group, and the G73 phosphate and ribose groups interact with Lys125 and Pro180.

As A76 of $_{cat}tRNA^{Asn}$ is located in the amidation active site, the crystal structure of the complex reflects an intermediate state between tRNA aspartylation and amidation of the esterified Asp. However, amidation of the β-carboxyl Asp occurs after activation by phosphorylation with ATP (Wilcox, 1969; Kern *et al*, 2005). Modelling of the ATP substrate in the GatB active site in the presence of $_{cat}tRNA^{Asn}$-bound Asp shows that the Asp moiety is 10 Å away from the γ-phosphate group of ATP (Nakamura *et al*, 2006) (Figure 5C and D). Furthermore, without moving the $_{cat}$tRNA-CCA end, the β-phosphoryl Asp points to the direction of the ammonia channel exit (Figure 5C and D), suggesting that the crystal structure represents the state between phosphorylation and amidation of the $_{cat}tRNA^{Asn}$-bound Asp. We therefore

Figure 2 SAXS measurements of the transamidosome. (**A**, **B**) SAXS *ab initio* modelling. The black curve represents the best fit from the *ab initio* modelling to the scattering data (circle). On the right, the average model is represented in black and the crystal structure, the 380-kDa molecule, composed of two dimeric ND-AspRSs (blue), two GatCABs (green, magenta and yellow for the GatC, A and B subunits), one $_{cat}tRNA^{Asn}$ (red) and one $_{scaf}tRNA^{Asn}$ (grey) is fitted to the SAXS average model. (**C**, **D**) Comparison of the crystal structure of the transamidosome to the experimental scattering data. (**C**) Crystal structure of the transamidosome depleted of one ND-AspRS bound on a $_{cat}tRNA^{Asn}$ and a $_{scaf}tRNA^{Asn}$. The two blue arrows are displayed to mark the different orientations of the GatCAB in the crystal structure compared with the model shown in panel E. (**D**) The circles represent the data and the curve represents the theoretical behaviour of the model calculated with CRYSOL. (**E**, **F**) Comparison of the model of the transamidosome to the experimental scattering data. (**E**) The model represents one ND-AspRS bound to two equivalent GatCABs and two $_{cat}tRNAs^{Asn}$. (**F**) The circles represent the data and the curve represents the theoretical scattering of the model calculated with CRYSOL. (**G**, **H**) SAXS rigid body refinement. (**G**) Best fit of the rigid body refinement performed using the SASREF program (black curve) to the scattering data (circles). (**H**) SASREF model. The flexible GatB C-t domain is in blue, the position of the C-t GatB in the crystal structure is in orange and the black arrow illustrates the movement of the GatB C-t domain in the absence of bound tRNA. The colour code is the same as in Figure 1.

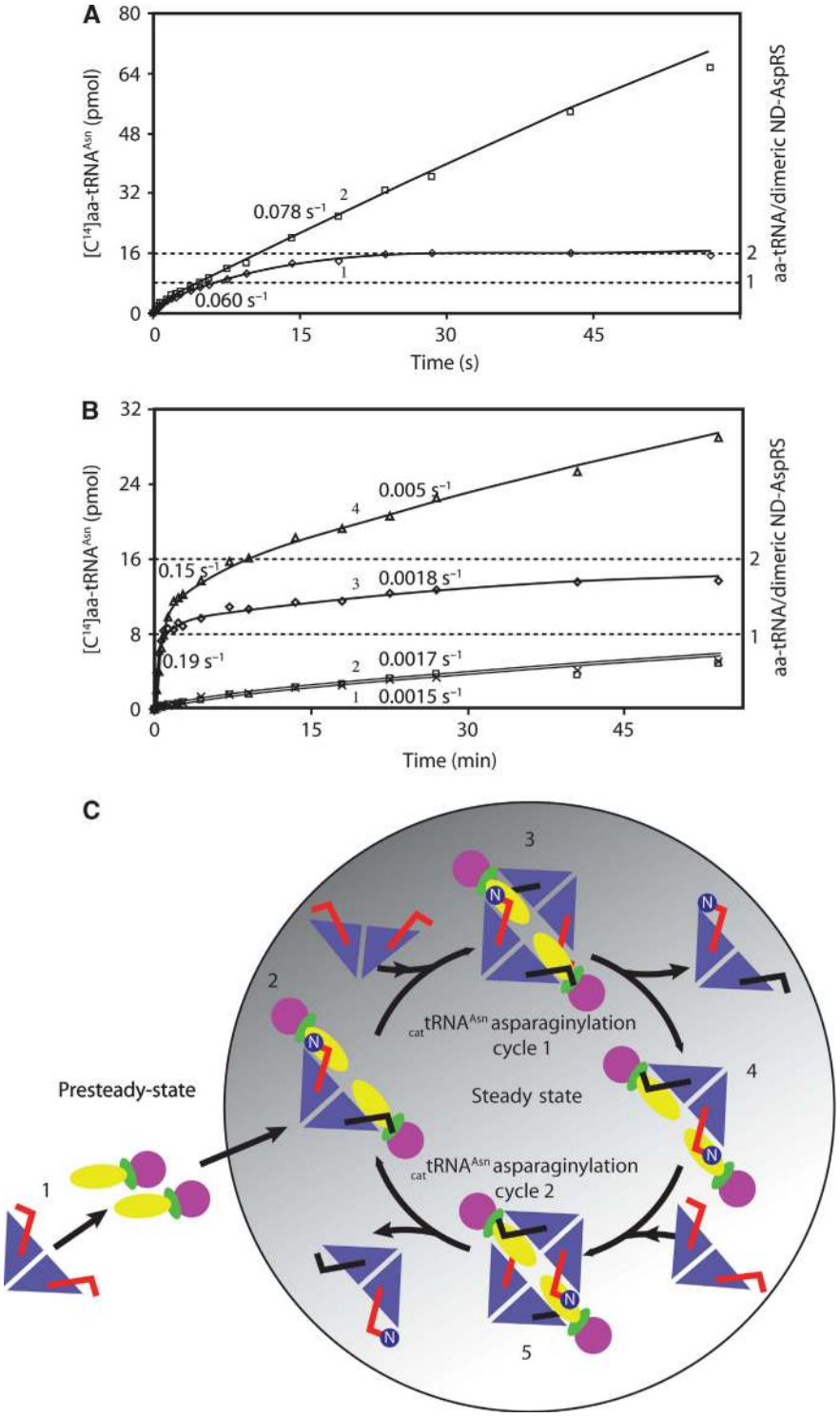

Figure 3 Presteady-state and steady-state aminoacylation kinetics of the ND-AspRS●tRNA^{Asn} complex and of the transamidosome and mechanism of transamidation. (**A**) Aminoacylation catalysed by the binary ND-AspRS●tRNA^{Asn} complex at 25°C. The reactions were conducted in the absence (1) or in the presence (2) of free tRNA^{Asn}. (**B**) Aminoacylation catalysed by the binary ND-AspRS●tRNA^{Asn} complex (1, 2) and by the transamidosome (3, 4) at 6°C in the presence of 25% glycerol. The reactions were conducted without (1, 3) or with (2, 4) free tRNA^{Asn}. The presteady-state and steady-state rate constants are indicated. (**C**) A proposed model of the dynamic of the presteady-state and steady-state functioning of the transamidosome. Two GatCABs (green ovals, magenta spheres and yellow ovals for the **C**, **A** and **B** subunits, respectively) bind the dimeric ND-AspRS (blue triangle) saturated by two tRNA^{Asn} (L forms) (1) and induces non-equivalence of the ND-AspRS active sites (2); only one tRNA ($_{cat}$tRNA^{Asn}) is functionally bound (red L) and is asparaginylated, whereas the other one ($_{scaf}$tRNA^{Asn}) not functionally bound (black L) promotes stability of the complex. This complex binds a second dimeric tRNA^{Asn}-bound ND-AspRS (3) promoting the dissociation of the ND-AspRS bound on the newly formed Asn-tRNA^{Asn} (4) that is replaced by a new ND-AspRS●tRNA^{Asn} complex (5). During this exchange, the $_{scaf}$tRNA^{Asn} bound on the second ND-AspRS by maintaining the transamidosome prevents its dissociation, whereas the bound $_{cat}$tRNA^{Asn} is asparaginylated. The dimeric AspRS bound on Asn-tRNA^{Asn} is then exchanged with a novel ND-AspRS●tRNA^{Asn} complex (cycle 2). Steady-state cycles 1 and 2 refer to successive asparaginylation of the $_{cat}$tRNA^{Asn} bound on each dimeric ND-AspRS. The letter N in the blue circles indicates asparaginylation of the $_{cat}$tRNA^{Asn}.

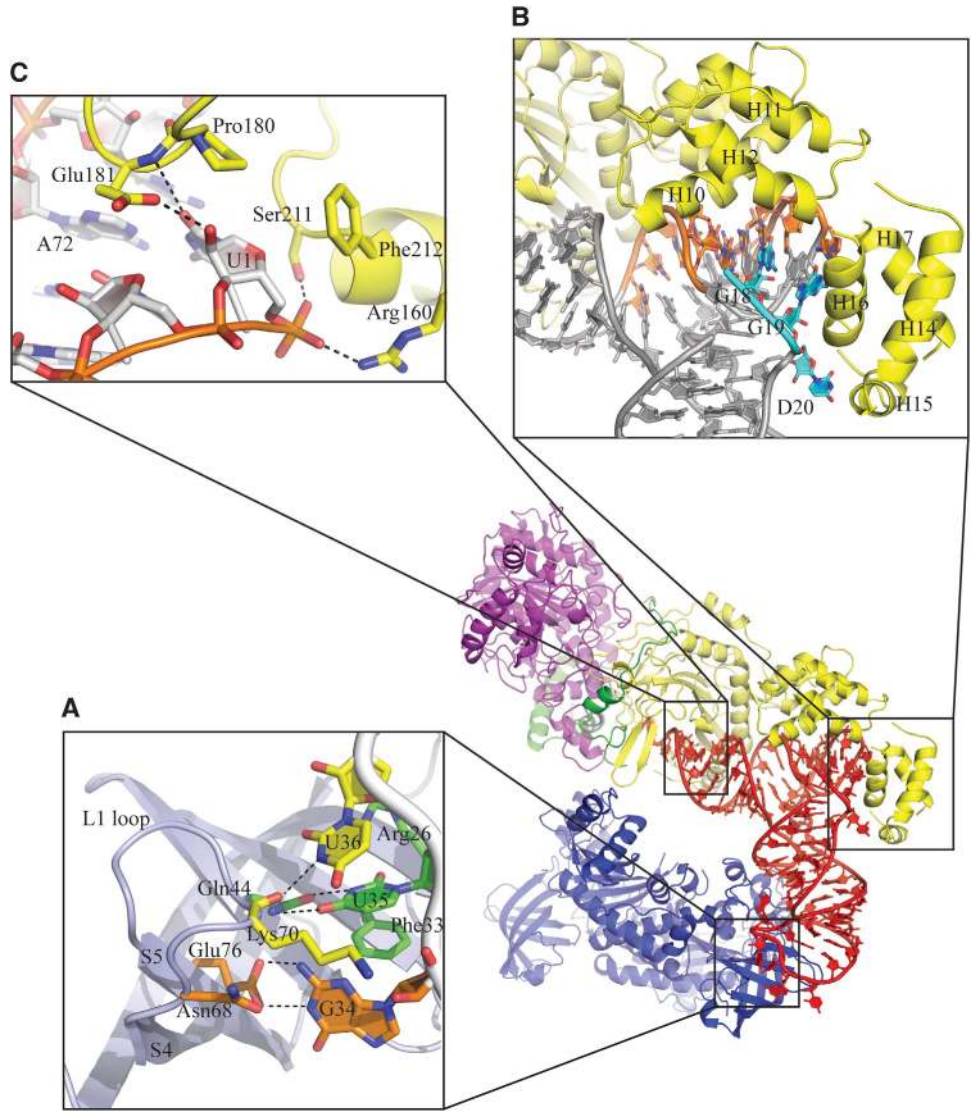

Figure 4 Recognition of $_{cat}$tRNA^{Asn} by the ND-AspRS and the GatB subunit of GatCAB. (**A**) Recognition of $_{cat}$tRNA^{Asn} anticodon by the ND-AspRS. The ABD is in light blue, the tRNA backbone is in light grey and the tRNA anticodon nucleotides 34, 35 and 36 are, respectively, in orange, green and yellow. The OB fold L1-loop between strands S4 and S5 is indicated. The aa are coloured according the nucleotide they contact. The black-dashed lines indicate hydrogen bonds. (**B**) Recognition of the $_{cat}$tRNA^{Asn} by the C-terminal domain of GatB. The tRNA^{Asn} D-loop is in blue and the T-loop and -arm in orange. The numbered H refers to the helix number. The GatB Yqey domain is formed by helices H14 to H17. (**C**) Recognition of nucleotide U1 of $_{cat}$tRNA^{Asn} by the GatB subunit. The aa residues contacting the base, the ribose and the phosphate groups are represented. The black-dashed lines indicate hydrogen bonds.

propose that after aminoacylation, the aspartylated end of $_{cat}$tRNA^{Asn} shifts from AspRS active site to the ATP site of GatB and that after activation, the β-phosphocarboxyl-Asp is located at the exit of the ammonia channel in position for a nucleophilic attack by ammonia (Figure 5E and F).

A scaffold tRNA^{Asn} mediates stability and integrity of the complex

$_{scaf}$tRNA^{Asn} is sandwiched between the ND-AspRS ABD and GatCAB (Figure 6). The electron density is clear from U1 to G73; however, the CCA end could not be traced. As for $_{cat}$tRNA^{Asn}, the anticodon stem, D and acceptor arms from $_{scaf}$tRNA^{Asn} are recognized by the ND-AspRS. The G34 and U35 bases establish H-bonds with, respectively, the carboxyl group of Glu76 and the carbonyl group of Lys70, whereas Phe33 is stacking the U35 base. The ring of U36 is recognized by Gln44 side chain, whereas O4 from its ribose group establishes H-bonds with the guanidinium group of Arg26 (Figure 6A). Moreover, Gly29 contacts C32 by Van der Waals interactions, whereas the O1 phosphate group and N6 from A38 establish H-bonds with Nε1 from the Trp24 side chain and the carbonyl group of Asp27 (Figure 6B). The acceptor arm of $_{scaf}$tRNA^{Asn} is bound at the interface of GatA and GatB subunits. The ribose residues of U3 and A72 contact the loop of GatA formed by residues 351–354 by Van der Waals interactions (Figure 6C). The G73 ring is stacked by Tyr95 from GatB and its N2 and O6 groups contact, respectively, the carboxyl and carbonyl groups of Asp96 and Tyr264 from GatB, whereas Tyr264 contacts the O6 from the base by its carbonyl group (Figure 6C). Interestingly, all the residues

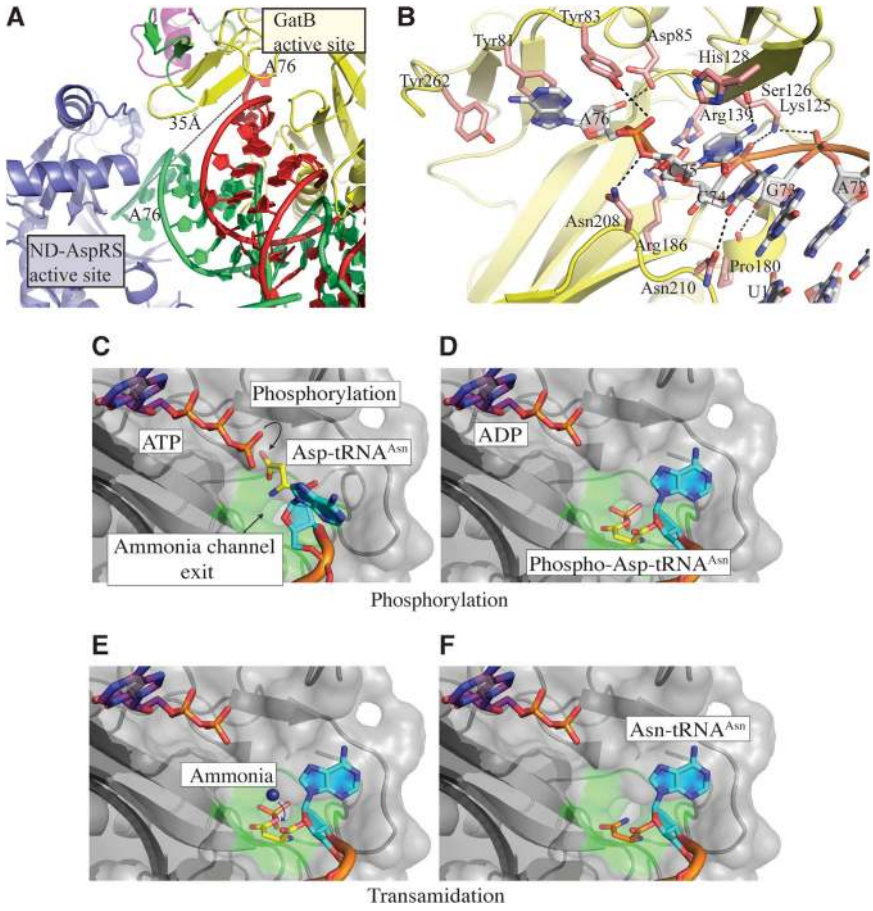

Figure 5 Interaction of the $_{cat}$tRNA^{Asn}-CCA end with the GatB catalytic site and mechanism of transamidation. (**A**) Model of the $_{cat}$tRNA^{Asn}-CCA switch. The ND-AspRS●tRNA complex was modelled by superposing the ND-AspRS bound to tRNA^{Asn} on the AspRS●tRNA^{Asp} complex from yeast (PDB code: 1ASY). tRNA^{Asp} is in green. The dashed line shows the distance between the binding sites of the tRNA terminal A76 in the ND-AspRS and in the GatB. (**B**) Recognition of the $_{cat}$tRNA^{Asn}-CCA end by the GatB active site. The GatB is in yellow cartoon and the tRNA-bound aa is in red salmon. $_{cat}$tRNA^{Asn} is shown as cartoon and sticks. The black-dashed lines indicate hydrogen bonds. (**C**–**F**) Models of β-carboxyl Asp phosphorylation and transamidation occurring in the GatB active site. ATP was modelled in the GatB active site using the structure of *S. aureus* GatCAB complexed with ADP-AlF4 as a reference (PDB code: 2G5I). tRNA is in orange ribbon, whereas the terminal A76 is in light blue. The Asp attached to the A76 3′OH ribose is in yellow stick. Except manual rotation of the A76, no further rearrangement was made on the structure. The GatB subunit is in grey ribbon and surface; the ammonia channel exit is delimited by the green area. (**C**) Putative position of the $_{cat}$tRNA^{Asn}-bound Asp prior its phosphorylation. (**D**) $_{cat}$tRNA^{Asn}-bound β-phosphocarboxyl-Asp at the exit of the ammonia channel. (**E**) Amidation of the activated β-carboxyl group of the bound Asp with ammonia (blue sphere) coming out from ammonia channel. (**F**) Formation of Asn-$_{cat}$tRNA^{Asn}; the Asn attached to the A76 3′OH ribose is in orange stick.

from GatA and GatB contacting the acceptor end of $_{scaf}$tRNA^{Asn} are well conserved among the species although they are not essential for catalysis. Four nucleotides of the D arm are contacted by the ND-AspRS mainly by their ribose and phosphate groups (Figure 6D). The O3 from G10 ribose and the phosphate of C11 are recognized by OH from the Tyr111 side chain. Recognition of C11 is strengthened by the interaction of its ribose group with the guanidinium group of Arg102. The Thr107 OH group and the main chain of Asn104 contact the U12 phosphate group, whereas the amide group of Asn104 main chain contacts the phosphate group of C13. Both N2 and O2 groups from, respectively, nucleotides G24 and C25 are contacted by the NH1 from Arg102 side chain, whereas O2 from the C25 ribose contacts the Oε1 of Glu95 and NH group of Lys98 side chain (Figure 6E). The phosphate group of C28 and the guanidinium group of Arg25 constitute the sole residues involved in recognition of the anticodon arm.

The transamidosome is essential for the GatCAB thermostability

T. thermophilus is a thermophilic eubacterium with optimal growth at 80–85°C. Therefore, proteins of this bacterium have to be thermostable. We studied the stability of the transamidosome components, free or in complex from 10 to 85°C using absorption measurements at 260 nm (Figure 6F). It is shown that tRNA^{Asn} is very stable, as its melting temperature (Tm) is 85°C. The ND-AspRS is thermostable up to 70°C but its thermostability increases when complexed to tRNA^{Asn}. In contrast, the GatCAB is poorly protected against heat inactivation, as its denaturation starts at 40°C. The presence of tRNA^{Asn} does not prevent denaturation of the GatCAB at the growth temperature of this thermophilic bacteria, as the denaturation starts at 50°C, in agreement with the low affinity of this substrate for the enzyme. Interestingly, when complexed in the transamidosome, the GatCAB becomes fully thermostable at 85°C.

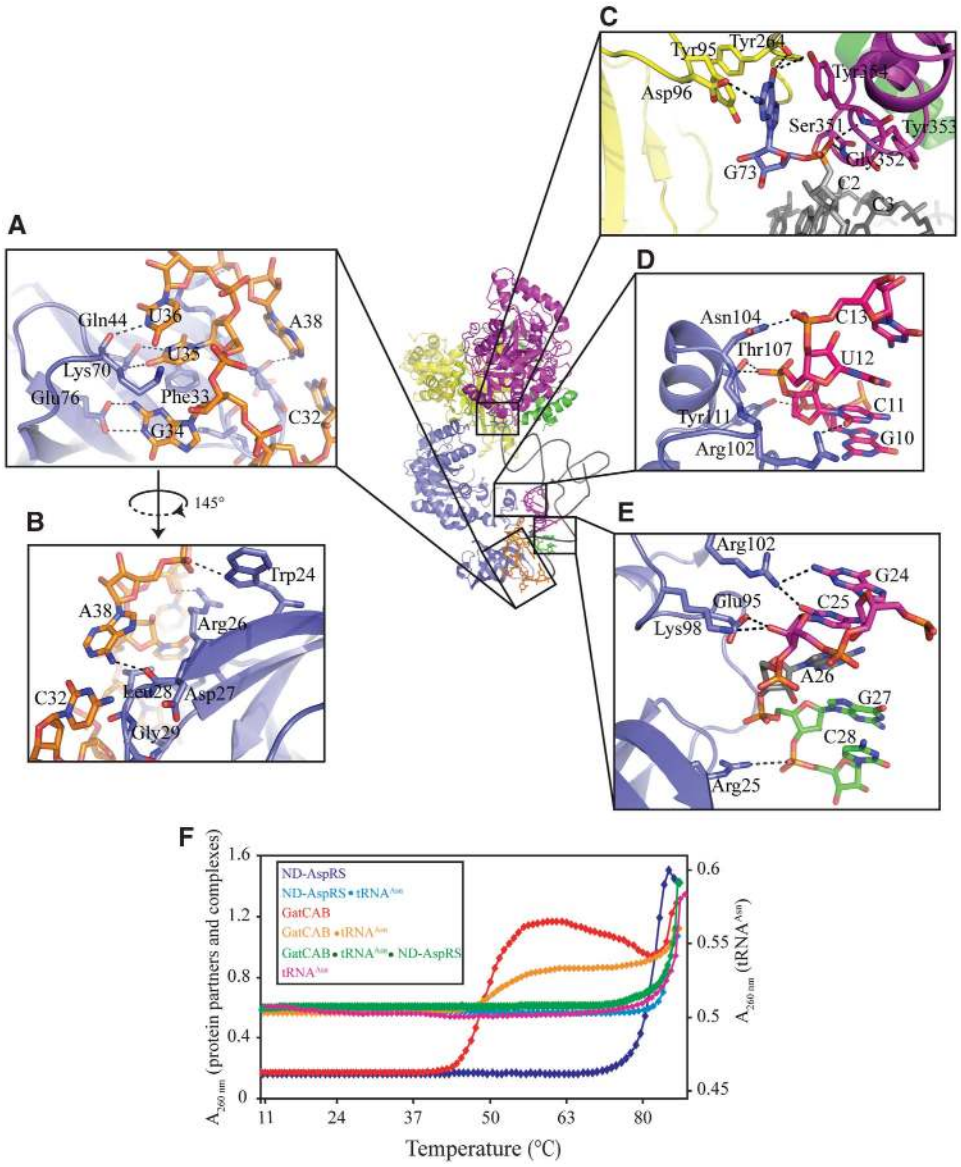

Figure 6 Stabilization of the transamidosome by the $_{scaf}$tRNA^{Asn}. (**A**–**E**) Recognition of the $_{scaf}$tRNA^{Asn} by the ND-AspRS (**A**, **B**, **D**, **E**), and the GatA and GatB subunits (**C**). The nucleotides from the anticodon, D arm and anticodon arm are, respectively, in orange, mangenta and green and the nucleotide G73 is in blue. (**F**) Stabilization of the protein partners of the transamidosome against thermal denaturation. The colour code is indicated in the insert. The same absorption (**A**) scale is used for the two proteins either in free state or inside the complex, but a different scale is used for the free tRNA^{Asn}.

Discussion

The transamidosome characterized in solution is a 380-kDa complex formed by a dimeric ND-AspRS bound to two tRNAs^{Asn} and two GatCABs. As, in addition to its function as substrate, the tRNA also acts as a scaffolding component, this complex constitutes a *bona fide* tRNP. One of the two tRNA^{Asn} of the dimeric ND-AspRS, $_{cat}$tRNA^{Asn}, is functionally bound and is devoted to asparaginylation, whereas the second one, $_{scaf}$tRNA^{Asn}, has the function of a scaffolding molecule that ensures the stability of the dynamic complex by preventing dissociation of the two GatCABs. By converting the $_{cat}$tRNA^{Asn}-bound Asp into Asn, the GatB subunit prevents release of Asp-$_{cat}$tRNA^{Asn} and constitutes the key component in the complex that maintains the integrity of the genetic code. Moreover, misincorporation of Asp into polypeptide chains is further prevented by an additional checkpoint promoted by the absence of significant affinity of the mischarged Asp-tRNA^{Asn} for the elongation factor EF-Tu (Becker and Kern, 1998; LaRiviere *et al*, 2001; Roy *et al*, 2007).

In the crystal structure, the acceptor end of the $_{cat}$tRNA^{Asn} is located in the GatB transamidation site. However, as tRNA must be charged with Asp by AspRS before transamidation, it can logically be assumed that formation of Asp-AMP by the ND-AspRS promotes binding of the tRNA CCA end in order to accept the activated Asp. Amidation of Asp occurs then after a shift of the aspartylated 3′ tRNA-CCA end of about 35 Å from ND-AspRS to the GatCAB. Interestingly, this movement resembles that occurring in the hydrolytic post-transfer correction mechanism when the mischarged 3′ end of tRNA shifts from the aaRS active site to the editing site (Nureki *et al*, 1998; Dock-Bregeon *et al*, 2004; Roy *et al*, 2004). It has

been shown that, in IleRS, the editing site is 34 Å away from synthetic site (Silvian *et al*, 1999).

$tRNA^{Asp}$ is capable of binding the ND-AspRS and even promoting formation of the ternary complex, albeit less efficiently than $tRNA^{Asn}$ (Bailly *et al*, 2007). Amidation of the bound Asp is, however, strongly disfavoured by the G1-C72 pair and the additional U20A of $tRNA^{Asp}$ both acting as antideterminants (Bailly *et al*, 2006). One may postulate that when the transamidosome is assembled with a dimeric ND-AspRS complexed to $tRNA^{Asn}$ on one subunit and $tRNA^{Asp}$ on the other one, $tRNA^{Asn}$ will bind functionally on the GatB site ($_{cat}tRNA^{Asn}$) but not $tRNA^{Asp}$ ($_{scaf}tRNA^{Asp}$), which therefore will escape asparaginylation. In any case, $tRNA^{Asp}$ will not be asparaginylated, as it cannot be aminoacylated in the transamidosome.

The crystal structure reveals that a particle of higher complexity than the 380-kDa one characterized in solution, can be formed, which contains an additional dimeric ND-AspRS bound to two $tRNAs^{Asn}$. As the two tRNA-bound ND-AspRSs are symmetrical, this particle very likely reflects a transient state of the transamidosome formed during steady state of tRNA asparaginylation. In this supramolecular complex, each dimeric ND-AspRS is bound to a $_{cat}tRNA^{Asn}$ whose CCA end is oriented towards the active site of one GatCAB and to a $_{scaf}tRNA^{Asn}$ whose terminal end is trapped at the GatA/GatB interface of the other GatCAB. Only the $_{cat}tRNA^{Asn}$ will be converted into Asn-$tRNA^{Asn}$. In the preformed transamidosome, the rate constant of asparaginylation of the first $_{cat}tRNA^{Asn}$ is probably determined by the shift of the aspartylated CCA end of the tRNA from AspRS to the GatCAB active site. Release of the asparaginylated $tRNA^{Asn}$ would dissociate the transamidosome and compromise GatCAB thermostability. Our study suggests that the kinetic mechanism has evolved to handle this paradox. We propose that after asparaginylation of the $_{cat}tRNA^{Asn}$, entering of a new $tRNA^{Asn}$ saturated ND-AspRS from the opposite side into the complex, promotes dissociation of the AspRS bound on Asn-$tRNA^{Asn}$. The new $_{cat}tRNA^{Asn}$ fits then into the active site of the previously non-functional GatCAB, whereas the new $_{scaf}tRNA^{Asn}$ inserts within the scaffolding site of the previously functional GatCAB. According to this mechanism, the steady-state rate of aspartylation/transamidation is determined by the exchange of the ND-AspRS bound to the freshly formed Asn-$tRNA^{Asn}$ with a new tRNA saturated ND-AspRS. During this exchange, the tRNP remains assembled by the $_{scaf}tRNA^{Asn}$ and $_{cat}tRNA^{Asn}$ of the second AspRS seen in the crystal structure (Figure 3C). After release of the ND-AspRS complex, Asn-$_{cat}tRNA^{Asn}$ is captured by EF-Tu to fuel the translation machinery.

Acquisition of thermal stability by the GatCAB only inside the transamidosome and, to a lesser extent by the ND-AspRS, to allow survival of *T. thermophilus* at its optimal growth temperature (80–85°C), is puzzling. It indicates that association of protein partners into multiprotein and nucleoprotein complexes can constitute an artifice developed by thermophilic organisms to confer thermal stability of their proteins at the optimal growth temperature. Because of its thermal instability, GatCAB may not derive from a thermostable protein ancestor but more likely from a mesophilic precursor. Likewise, the ND-AspRS, less thermostable than the discriminatory AspRS from *T. thermophilus*, is probably not of thermophilic origin and may also derive from a mesophilic organism.

Materials and methods

Purification, crystallization and structure determination of the transamidosome

The methods were described earlier (Bailly *et al*, 2007, 2008, 2009). Data and refinement statistics are summarized in Table I. The structure and the structure factors have been deposited to the Protein Data Bank under the accession number 3KFU.

SAXS experiments

The measurements were carried out on a laboratory-based instrument at the University of Aarhus (Pedersen, 2004). Concentration series of c and c/2 were measured for 3 h at 4°C. Background subtraction and normalizations were performed by use of the SUPERSAXS package (CLP Oliveira and JS Pedersen, unpublished data). The data were normalized to absolute scale by use of water as a primary standard and the final intensity was displayed as a function of the scattering vector $q = (4\pi/\lambda)\sin(\theta)$, where $\lambda = 1.54$ Å is the X-ray wavelength and θ is the angle between the incoming and the scattered X-rays. The *ab initio* modelling and comparison with crystal structure data were carried out with, respectively, the DAMMIN (Svergun, 1999) and CRYSOL (Svergun *et al*, 1995) programs. Rigid body modelling using subunits with known atomic structure were carried out using SASREF (Svergun *et al*, 1995). The optimization of the *ab initio* and rigid body models has been done using simulated annealing procedures. All averaging of the models were carried out using the DAMAVER program package (Kozin and Svergun, 2001).

Aminoacylation and transamidation reactions

The reactions were conducted in 200 μl mixtures containing 0.1 M Hepes-Na buffer pH 7.2, 30 mM KCl, 2 mM $MgCl_2$ 0.4 μM of either binary AspRS•$tRNA^{Asn}$ complex or transamidosome isolated by gel filtration, 10 μM L-[^{14}C] Asp (330 c.p.m./pmol), 1 mM ATP, 2 mM L-Gln without or with 5 μM $tRNA^{Asn}$. The [^{14}C] aa-tRNA formed at the indicated temperature was determined as described (Bailly *et al*, 2007) in 20 μl aliquots withdrawn at various incubation times.

Thermal denaturation

Thermal denaturation assays were performed with an Uvikon XL (SECOMAM, Domont, France) spectrophotometer equipped with a Peltier thermostated cell holder. Denaturation curves were recorded at 260 nm with a heating rate of 0.25°C/min between 10 and 85°C. The temperature was measured by a thermocouple inserted into one cell. Cells were designed specifically by Dr P Walter (IBMC, Strasbourg), in order to prevent any water loss by evaporation during the experiment. Experiments were carried out in 0.1 M Hepes-Na buffer pH 7.2 containing 30 mM KCl, 2 mM $MgCL_2$ in the presence of the partners of the transmidosome in various states and in a stoichiometry found in the ternary complex: 0.8 μM $tRNA^{Asn}$ or GatCAB or purified GatCAB•$tRNA^{Asn}$ complex or ND-AspRS subunits, or 0.4 μM purified transamidosome or ND-AspRS•$tRNA^{Asn}$ complex.

The figures of the structure of the transamidosome were generated with Pymol. DeLano WL. The PyMOL Molecular Graphics System (2002) on World Wide Web http://www.pymol.org.

Supplementary data

Supplementary data are available at *The EMBO Journal* Online (http://www.embojournal.org).

Acknowledgements

This work was supported by the University Louis Pasteur (Strasbourg), the Centre National de la Recherche Scientifique (CNRS), the Association pour la Recherche sur le Cancer (ARC), ACI Biologie Cellulaire Moléculaire et Structurale and the Center for Carbohydrate Recognition and Signalling (CARB). We thank E Westhof, P Nissen and J Stougaard for support, L Yatime and JP Morth for discussions, E Ennifar for help with UV-melting experiments, M Brayé for technical assistance and LE Sanderson for critical reading of the paper. M Bailly and M Blaise were recipients of a fellowship from ARC and AFM.

Author contributions: M Blaise crystallized, solved the structure, designed research and wrote the paper, M Bailly purified the complex and participated to the first crystallizations, M Bailly and

F Fischer performed the biochemical experiments, M Frechin helped with the structure rebuilding, MA Behrens did the SAXS measurements and SAXS data analysis, CPL Oliveira, JS Pedersen supervised the SAXS experiments and data analysis, S Thirup supervised research, H Becker and D Kern supervised research and wrote the paper.

Author information: Atomic coordinates and structure factors have been deposited with the Protein Data Bank under accession 3KFU.

Conflict of interest

The authors declare that they have no conflict of interest.

References

Bailly M, Blaise M, Lorber B, Becker HD, Kern D (2007) The transamidosome: a dynamic ribonucleoprotein particle dedicated to prokaryotic tRNA-dependent asparagine biosynthesis. *Mol Cell* **28:** 228–239

Bailly M, Blaise M, Lorber B, Thirup S, Kern D (2009) Isolation, crystallization and preliminary X-ray analysis of the transamidosome a ribonucleoprotein involved in asparagine formation. *Acta Crystallogr Sect F Struct Biol Cryst Commun* **65:** 577–581

Bailly M, Blaise M, Roy H, Deniziak M, Lorber B, Birck C, Becker HD, Kern D (2008) tRNA-dependent asparagine formation in prokaryotes: characterization isolation and structural and functional analysis of a ribonucleoprotein particle generating Asn-tRNA^{Asn}. *Methods* **44:** 146–163

Bailly M, Giannouli S, Blaise M, Stathopoulos C, Kern D, Becker HD (2006) A single tRNA base-pair mediates bacterial tRNA-dependent biosynthesis of asparagine. *Nucleic Acids Res* **34:** 6083–6094

Becker HD, Kern D (1998) *Thermus thermophilus*: a link in evolution of the tRNA-dependent amino acid amidation pathways. *Proc Natl Acad Sci USA* **95:** 12832–12837

Charron C, Roy H, Blaise M, Giegé R, Kern D (2003) Non-discriminating and discriminating aspartyl-tRNA synthetases differ in the anticodon-binding domain. *EMBO J* **22:** 1632–1643

Curnow AW, Ibba M, Söll D (1996) tRNA-dependent asparagine formation. *Nature* **382:** 589–590

Curnow AW, Tumbula DL, Pelaschier JT, Min B, Söll D (1998) Glutamyl-tRNA^{Gln} amidotransferase in *Deinococcus radiodurans* may be confined to asparagine biosynthesis. *Proc Natl Acad Sci USA* **95:** 12838–12843

Delarue M, Poterszman A, Nikonov S, Garber M, Moras D, Thierry J-C (1994) Crystal structure of a prokaryotic aspartyl-tRNA-synthetase. *EMBO J* **13:** 189–197

Deniziak M, Sauter C, Becker HD, Paulus CA, Giegé R, Kern D (2007) *Deinococcus* glutaminyl-tRNA synthetase is a chimer between proteins from an ancient and the modern pathways of aminoacyl-tRNA formation. *Nucleic Acids Res* **35:** 1421–1431

Dock-Bregeon AC, Rees B, Torres-Larios A, Bey G, Caillet J, Moras D (2004) Achieving error-free translation; the mechanism of proofreading of threonyl-tRNA synthetase at atomic resolution. *Mol Cell* **16:** 375–386

Ibba M, Söll D (2004) Aminoacyl-tRNAs: setting the limits of the genetic code. *Genes Dev* **18:** 731–738

Kern D, Lapointe J (1979) Glutamyl-transfer ribonucleic acid synthetase from *Escherichia coli*. Effect of alteration of the 5-(methylaminomethyl)-2-thiouridine in the anticodon of glutamic acid transfer ribonucleic acid on the catalytic mechanism. *Biochemistry* **18:** 5819–5826

Kern D, Roy H, Becker H (2005) Asparaginyl-tRNA synthetases. In *The Aminoacyl-tRNA Synthetases*, Ibba M, Francklyn C, Cusack S (eds), Chapter 28, Georgetown, TX: Landes Bioscience

Kozin MB, Svergun DI (2001) Automated matching of high- and low-resolution structural models. *J Appl Cryst* **34:** 33–41

LaRiviere FJ, Wolfson AD, Uhlenbeck OC (2001) Uniform binding of aminoacyl-tRNAs to elongation factor Tu by thermodynamic compensation. *Science* **294:** 165–168

Nakamura A, Sheppard K, Yamane J, Yao M, Söll D, Tanaka I (2010) Two distinct regions in *Staphylococcus aureus* GatCAB guarantee accurate tRNA recognition. *Nucleic Acids Res* **38:** 672–682

Nakamura A, Yao M, Chimnaronk S, Sakai N, Tanaka I (2006) Ammonia channel couples glutaminase with transamidase reactions in GatCAB. *Science* **312:** 1954–1958

Nureki O, Vassylyev DG, Tateno M, Shimada A, Nakama T, Fukai S, Konno M, Hendrickson TL, Schimmel P, Yokoyama S (1998) Enzyme structure with two catalytic sites for double-sieve selection of substrate. *Science* **280:** 578–582

Oshikane H, Sheppard K, Fukai S, Nakamura Y, Ishitani R, Numata T, Sherrer RL, Feng L, Schmitt E, Panvert M, Blanquet S, Mechulam Y, Söll D, Nureki O (2006) Structural basis of RNA-dependent recruitment of glutamine to the genetic code. *Science* **312:** 1950–1954

Pedersen JS (2004) A flux- and background-optimized version of the NanoSTAR small-angle X-ray scattering camera for solution scattering. *J Appl Cryst* **37:** 369–380

Roy H, Becker HD, Mazauric MH, Kern D (2007) Structural elements defining elongation factor Tu mediated suppression of codon ambiguity. *Nucleic Acids Res* **35:** 3420–3430

Roy H, Ling J, Irnov M, Ibba M (2004) Post-transfer editing *in vitro* and *in vivo* by the beta subunit of phenylalanyl-tRNA synthetase. *EMBO J* **23:** 4639–4648

Ruff M, Krishnaswamy S, Boeglin M, Poterszman A, Mitschler A, Podjarny A, Rees B, Thierry J-C, Moras D (1991) Class II aminoacyl transfer RNA synthetases: crystal structure of yeast aspartyl-tRNA synthetase complexed with tRNA^{Asp}. *Science* **252:** 1682–1689

Schmitt E, Moulinier L, Fujiwara S, Imanaka T, Thierry JC, Moras D (1998) Crystal structure of aspartyl-tRNA synthetase from *Pyrococcus kodakaraensis* KOD: archaeon specificity and catalytic mechanism of adenylate formation. *EMBO J* **17:** 5227–5237

Sheppard K, Yuan J, Hohn MJ, Jester B, Devine KM, Söll D (2008) From one amino acid to another: tRNA-dependent amino acid biosynthesis. *Nucleic Acids Res* **36:** 1813–1825

Silvian LF, Wang J, Steitz TA (1999) Insights into editing from an Ile-tRNA synthetase structure with tRNA^{Ile} and mupirocin. *Science* **285:** 1074–1077

Small-Howard A, Morozova N, Stoytcheva Z, Forry EP, Mansell JB, Harney JW, Carlson BA, Xu X-M, Hatfield DL, Berry MJ (2006) Supramolecular complexes mediate selenocysteine incorporation *in vivo*. *Mol Cell Biol* **26:** 2337–2346

Svergun DI (1999) Restoring low resolution structure of biological macromolecules from solution scattering using simulated annealing. *Biophys J* **76:** 2879–2886

Svergun DI, Barberato C, Koch MHJ (1995) CRYSOL—a program to evaluate X-ray solution scattering of biological macromolecules from atomic coordinates. *J Appl Cryst* **28:** 768–773

Svergun DI, Petoukhov MV (2005) Global rigid body modeling of macromolecular complexes against small-angle scattering data. *Biophys J* **89:** 1237–1250

Tomita K, Ishitani R, Fukai S, Nureki O (2006) Complete crystallographic analysis of the dynamics of CCA sequence addition. *Nature* **443:** 956–960

Wilcox M (1969) Gamma-glutamyl phosphate attached to glutamine-specific tRNA a precursor of glutaminyl-tRNA in *Bacillus subtilis*. *Eur J Biochem* **11:** 405–412

Wu J, Sheppard K, Kitabatake M, Kwon ST, Söll D, Smith JL (2009) Insights into tRNA-dependent amidotransferase evolution and catalysis from the structure of the *Aquifex aeolicus* enzyme. *J Mol Biol* **391:** 703–716

Zhang C-M, Liu C, Slater S, Hou YM (2008) Aminoacylation of tRNA with phosphoserine for synthesis of cysteinyl-tRNA^{Cys}. *Nat Struct Mol Biol* **15:** 507–514